Zeolite Encapsulated Ni(II) and Cu(II) Complexes with Tetradentate N2O2 Schiff Base Ligand: Catalytic Activity Towards Oxidation of Benzhydrol and Degradation of Rhodamine-B

SCHOLARONE™
Manuscripts

Zeolite Encapsulated Ni(II) and Cu(II) Complexes with Tetradentate N₂O₂ Schiff Base Ligand: Catalytic Activity Towards Oxidation of Benzhydrol and Degradation of Rhodamine-B

G. Ramanjaneya Reddy,[a] S. Balasubramanian,[a] K. Chennakesavulu[b] *

[a]Department of Inorganic Chemistry, School of Chemical Sciences, University of Madras, Guindy Campus, Chennai-600 025, India.
[b]Department of Chemistry and International Research Centre, Sathyabama University, Jeppiaar Nagar, Chennai - 600 119, India..
*Corresponding author: chennanml@yahoo.com, gonturamunom@gmail.com.
Tel.: +91 9994228166, 044 22202794.

Abstract

The nickel (II) and copper (II) complexes of the Schiff base ligand O, O'-trimethyl bis (salicylidene isonicotinylhydrazone)(H$_2$L) were synthesized and characterized. The encapsulation of these complexes in the cavities of zeolite was achieved by a fixed ligand method (FLM). The free complexes (FC) and the retention of zeolite encapsulated metal complexes (i.e Ni(II)L-Y, Cu(II)L-Y) (ZEMC) were studied by several spectroscopic, thermal analysis, sorption and microscopic techniques (FTIR, NMR, ESI-mass, Conductivity, DRS/UV-Vis, EPR, XPS, AAS, TGA, XRD, Nitrogen isotherm, Magnetic and (SEM/TEM)EDX). This studies reveals the formation and stability of the metal complexes in the cavities of zeolite. The catalytic activity of free complexes and encapsulated complexes was studied in liquid phase oxidation of the benzhydrol/H$_2$O$_2$ and photo degradation of rhodamine-B (RhB) under UV/Visible(H$_2$O$_2$) irradiations. The catalytic activity of benzhydrol (BH) oxidation and RhB degradation was higher with free complexes and encapsulated complexes respectively. In most of the cases the copper (II) (Cu(II)L.2ClO$_4$,Cu(II)L-Y) complexes was shown better activity of than nickel (II) complexes (Ni(II)L.2ClO$_4$,Ni(II)L-Y) in both BH and RhB degradation reactions. The enhancement of the Cu(II)L-Y activity mainly due to the metal percentage was present in cavities and surfacearea. Hence in the case of FC the copper (II) complexes rate of the reaction (% of conversion) is more than nickel (II) in BH

30   oxidation but in the case of ZEMC the photocatalytic activity and rate of the reaction (% of

31   conversion) more for Cu(II)L-Y than Ni(II)L-Y. These results show the both oxidation

32   reactions follow the pseudo first order kinetics. The catalytic activity of the recovered and

33   purified ZEMC checked with the fresh catalyst.

34   **Keywords**: N_2O_2 Schiff base, Nickel (II), Copper (II), Fixed ligand method, Benzhydrol

35   oxidation, Rhodamine-B.

36   **1. Introduction**

37   Transition metal complexes play a vital role in the field of catalysis and photocatalysis

38   i.e. liquid phase oxidation, reduction and polymerization etc.[1-3] The recovery and separation of

39   transition metals from the products in homogeneous medium (e.g. hydrocarbons, aliphatic

40   alcohols, alkyl benzenes, amides, amines, aliphatic carboxylic acids, thioethers and xanthene

41   class of dyes, etc) are challenging tasks. In order to overcome this difficulty, the research

42   interest in the heterogeniation of homogenous catalyst was raised.[4,5] However the enhancement

43   of catalyst activity with the nickel (II) and copper (II) based systems was alternative to the

44   highly expensive metals like ruthenium, palladium. Hence, the impregnation of homogeneous

45   transition metal complexes into solid support such as polymer, zeolite and MCM41 was

46   attempted.[6] The zeolites are made up of the aluminosilicates named as "solid acid" and it is

47   further alternative to commercially available toxic acids such as sulphuric acid, potassium

48   dichromate, nitric acid**.** The zeolite Na-Y is an exchange bowl and interesting material due to

49   its low cost and an intra crystalline cavity which was suitable the transition metal ions

50   exchange. The exchange and encapsulation ability of the metal complexes within the cavities of

51   supercages depends on the Na^+ ion and size of the zeolite host.[7] Hence the encapsulation

52   (heterogeniation) of the metal complexes (homogeneous) within the supercages can used for

53   the effectively in the photo (chemical) oxidation reactions. The modified catalyst has more

54 advantages than those homogeneous counter points. This can be act as effective ecofriendly

55 catalyst to convert high toxic pollutants to the very less toxic minerals.

56   The modified zeolite can delocalise the band gap excited electrons of HOMO and

57 LUMO levels of metal complexes. Hence they minimize the electron-hole recombination

58 besides a relative number of active sites present on the high surface area based solid supports.

59 In addition, ability of the modified zeolite favours photo induced electron-transfer reactions and

60 generate the photo active powerful oxidative ion-radical species like $^{\bullet}OH$, $^{-}O_2$, $^{+\bullet}O_2H$. The

61 modified zeolite with green oxidant 30% H_2O_2 can enhance the photo catalytic performance of

62 various dyes (RhB, methyl orange, cango red) by generation of a most power full oxidant(E_o=

63 $^{\bullet}OH$ (E^o =2.8 V) than other oxidants.[8] These supported systems improves the rate of the

64 reaction and catalytic activity towards the decolourisation of the carcinogenic xanthenes (azo)

65 class of dyes and oxidation of the aryl alchohols.[9] Since, the photo degradation of dyes is an

66 important and also very few reports are available to removes the xanthene class of dyes by

67 using the pure and supported Schiff base hydrazones complexes**.[10]**

68   The metal complexes of aryl hydrazones have good biological and catalytic

69 significances, because of the tetradentate (dioxa diaza) moiety owing their chelating ability

70 with the metal ions. In the liquid phase oxidation reactions, whose type of metal hydrazone

71 analogues with the nickel (II) and copper (II) exchange zeolite was rarely reported.[11] The

72 synthesis and extensive studies of the acyclic tetradentate N_2O_2 Schiff base ligand O, O'-

73 trimethyl bis (salicylidene isonicotinoyl hydrazone) with Ni(II), Cu(II) and its corresponding

74 encapsulated complexes by FLM in the cavities of zeolite and its usage in BH oxidation and

75 degradation of RhB dyes were not established.[12]

76   In the present study, an attempt was made on the synthesis of the Schiff base ligand O,

77 O'-trimethyl bis(salicylidene isonicotinoyl hydrazone) (H_2L) by the condensation between 1, 3-

78 Bis(2-carboxyaldehydephenoxy)propane(SAL) and isonicotinyl hydrazine (INH) in presence of

79   the perchlorates of the Ni(II) and Cu(II). The metal complexes are encapsulated in the cavities

80   of zeolite by FLM.[12] The catalytic activity of the synthesised materials were tested in the liquid

81   phase oxidation of BH and the photo degradation of RhB. The spectrophotometric technique

82   was used for determination of the products and catalytic activity of the composite materials.

83   **2. Experimental**

84   **2.1 Materials**

85   The chemicals salicylaldehyde, 1, 3 dibromo propane, Isonicotinylhydrazide, Zeolite-Y

86   (Si/Al= 2.7, $Na_{52}[(AlO_2)_{52}(SiO_2)_{140})]$, Benzhydrol, Hydrogen peroxide (30 %), Rhodamine-B

87   were obtained from Sigma Aldrich. The Milli-Q water was used during the experimental work.

88   **2.2 Physicochemical measurements and characterization**

89   The NMR spectra were recorded on Bruker Avance 400MHz NMR spectrometer, the

90   ESI mass spectral data were obtained using ESI-MS Thermo Finnigan LCQ model advantage

91   MAX 6000ESI spectrometer, the FTIR spectra were recorded on a FTIR Perkin-Elmer 8300

92   spectrometer with the KBr disk and the UV-Visible Diffuse Reflectance Spectral (UV-Vis

93   DRS) analyses were carried on a Perkin-Elmer lambda-650 DRS UV-visible

94   spectrophotometer. The UV–Vis absorption spectra using a Perkin Elmer Lambda-35

95   spectrophotometer operating in the range 200-800 nm for liquid samples. Conductivity

96   measurements were carried out in mmol solutions of the metal complexes in DMSO. The EPR

97   spectrum of the copper (II) complex was recorded at LNT on a Varian E-4 X-band

98   spectrometer using TCNE as the g-marker (2.0023). XPS analyses were carried out on

99   XM1000 Omicron nanotechnology XPS system with Al-Kα monochromatic wavelength. The

100   FC and ZEMC samples were made into pellets and were used as such for X-ray Photoelectron

101   Spectroscopic (XPS) analysis. The high resolution XPS traces were deconvoluted using the

102   Gaussian and Lorentzian statistical analysis by using origin-7 software. The crystalline nature

103   of the FC and ZEMC was ascertained by the powder X-ray diffraction using Bruker D8

104   advance diffractometer with monochromatic Cu-Kα_1 radiation (λ=1.5418 A°). After completely

105   destroying the zeolitic frame work with hot HCl, the nickel and copper percentage were

106   analyzed by atomic absorption spectrophotometer (AAS, Perkin-Elmer 4100-1319) and SiO_2

107   was determined by gravimetric analysis. TGA experiments were performed with Versa Therm

108   Cahn thermo balance TG-151 with a sensitivity of 10 μg. TGA experiments were conducted in

109   the temperature range of 300-1200 K with 20 ± 0.01 mg of the samples and the analyses were

110   carried out at a heating rate of 10 K/min under static air atmosphere. The N_2 adsorption,

111   desorption isotherms and Brunauer-Emmett-Teller (BET) specific surface area measurements

112   at 77K were carried out on Micrometrics ASAP (Model 2020) surface area analyzer with the

113   nitrogen and helium gases with a purity of 99.99%. The scanning electron micrograph (SEM)

114   was obtained using HITACHI-S3690 scanning electron microscope. HRTEM analysis was

115   carried out by using a FEI TECNAI G2 (T-30) transmission electron microscope with an

116   accelerating voltage of 250 KV. The average particle size was measured by the Image-J soft

117   ware tool. The products in one the BH oxidation were analyzed by LC-MS technique using

118   Agilent 6110 LC-MS ESI mode with carvacrol use as internal standard.

119   **2.3 Preparation of the 1, 3-Bis (2-carboxyaldehydephenoxy) propane (SAL)**

120   Salicyladehyde (0.61g, 5 mmol) was dissolved in   20 mL DMF and potassium

121   corbonate (1.73 g, 12.5 mmol) was added and mixture was stirred at room temperature and 1,3

122   dibromopropane (0.51g, 2.5 mmol) was added drop wise and then the reaction mixture was

123   stirred under reflux for 6 h. The resulted mixture was partitioned between water and

124   ethylacetate, the ethyl acetate layer was collected and concentrated under reduced pressure and

125   then subjected to silica gel 100-200 mesh column chromatography using 1:9 hexane-

126   ethylacetate as eluent to afford compounds(1.07g 75%) in pure form. the purified SAL was

127   characterized and the results are well matched with earlier reported method.[13]. **(ESI: S35)** [1]H

128   NMR (CDCl$_3$, 500 MHz): δ: 2.43 (2H, p, OCH$_2$CH$_2$CH$_2$O), 4.33 (4H, t, J = 7.6 Hz,

129   O$\underline{CH_2}$CH2$\underline{CH_2}$O), 7.03 (4H, m, Ar-H), 7.55 (2H, t, J = 7.7 Hz, Ar-H), 7.83 (2H, d, J = 7.7 Hz,

130   Ar-H), 10.49 (2H, s, Aldehyde-H); ^{13}C NMR (CDCl$_3$, 125 MHz) **(ESI: S36)**: δ 29.2, 64.7,

131   112.5, 121.0, 124.9, 128.8, 136.2, 161.0, 189.6.

132   2.4 Preparation of the O, O'-trimethyl bis (salicylidene isonicotinoyl hydrazine (H$_2$L)

133   The O, O'-trimethyl bis (salicylidene isonicotinyl hydrazone) was prepared by refluxing

134   the aliquot of the SAL (1.12 g, 2 mmol), isonicotinyl hydrazide (1.8 g, 4 mmol), two drops of

135   the glacial acetic acid in absolute ethanol (40 mL) for 2 h, the resulting white solid was washed

136   with the water, ethanol, chloroform, diethyl ether and dried under vacuum Yield:0.68 g (80%).

137   M.p. 521-523 K. ESI-mass: m/z 545.27 (M+Na).^{1}HNMR (DMSO-d6,400MHz) ppm: 12.02 (s,

138   2H, amide NH), 9.01-8.42 (m, 6H, Ar-H and imine CH), 8.07-7.53 (m, 6H, Ar-H), 7.37 (s, 2H,

139   Ar-H), 7.11 (s, 2H, Ar-H), 6.98 (s, 2H, Ar-H), 4.27 (s, 4H, O$\underline{CH_2}$) and 2.26 (s, 2H,

140   O$CH_2$$\underline{CH_2}CH_2$O); ^{13}C NMR (DMSO-d6, 80 MHz) ppm: 162.08, 157.57, 150.77, 149.99,

141   144.91, 141.02, 132.37, 126.27, 123.60, 122.68, 122.03, 121.41, 113.26, 65.30 and 29.26.

142   UV/Vis (DMSO): λ_{max} (ε:cm^{-1} mol^{-1} L) =272 (56600), 288 (58577) and 332(6658).

143   2.5 Preparation of Ni(II)L . 2ClO$_4$

144   To the DMF solution (5 mL) of (H$_2$L) (0.52 g, 1 mmol), the 30 mL ethanolic solution of

145   nickel perchlorate hexahydrate (0.38 g, 0.5 mmol) were added and then heated at 353 K for 3 h.

146   The resulting lemon yellow solid was washed with the hot water, methanol, diethyl ether and

147   dried under vacuum.Yield:0.6g (72%), M.p. and decomposition > 543 K; ESI-mass m/z 579.2.

148   λ_{max} = 260 nm (ε =14050 cm^{-1}mol^{-1} L), 368 nm (ε =18990 cm^{-1}mol^{-1} L), 670 nm (ε = 68 cm^{-1}

149   mol^{-1} L^{-1}). Molar conductivity (Λ) =14.5 mho cm^{-2} mol^{-1}.

150   2.6 Preparation of Cu(II)L. 2ClO$_4$

151   To the DMF solution (5 mL) of H$_2$L (1.1 g, 0.5 mmol), 30 mL ethanolic solution of

152   copper perchlorate hexahydrate (0.36 g, 0.5 mmol) were added and heated at 353 K for 3 h.

153   The resulting olive green solid was washed with the hot water, methanol, and diethyl ether and

154   dried under vacuum. Yield: 0.7g (80 %) M.p. and decomposition > 513 K; MS: m/z 585. $\lambda_{max} =$

155   270 (ε =14829 cm^{-1} mol^{-1}L), 368 nm (ε =19300 cm^{-1}mol^{-1}L), 685 nm (ε =33 cm^{-1}mol^{-1}L). Molar

156   conductivity (Λ) = 11.8 mho cm^2 mol^{-1}.

157   **2.7 Preparation of metal exchanged zeolite, (M(II)-Y [M=Ni(II) and Cu(II)])**

158   The metal perchlorate (M(ClO$_4$).6H$_2$O, 0.1 mmol) was added to the 50 mL aqueous

159   solution of 1 g of Na-Y zeolite and it was stirred for 8 h at 368 K. The obtained solids were

160   filtered, washed with 100 mL of hot distilled water and dried under vacuum for 10 h at 353 K.

161   **2.8 Preparation of the metal hydrazone Schiff base complexes in the zeolite (M(II)L-Y)**

162   **via FLM.**

163   Preparation of the Schiff base aryl hydrazone metal complexes in the cavities of the

164   zeolite was achieved by heating at 333 K in DMF/methanolic solution of **H$_2$L** with the **M(II)-Y**

165   for 8 h. The resulting solids were washed with the hot DMSO (10 mL), water and dried for 12

166   h. The solids were soxhlet extracted with the ethanol and acetonitrile/DMF 6 and 24 h

167   respectively to remove excess unreacted starting materials adsorbed onto the external surface of

168   the zeolite crystalline. The resulting solids were dried at 253 K under vacuum for 24 h. Yield:

169   0.3-0.34 g. Colour: [Ni(II)L-Y] (pale yellow), [Cu(II)L-Y] (pale green).

170   **2.9. Oxidation of the BH by the FC and ZEMC.composite materials**

171   A mixture of the M(II)L.2ClO$_4$ (0.5 mg 0.01 mmol) (100 mg in case of ZEMC), 30%

172   hydrogen peroxide (0.34 g, 1mmol) and BH (0.0184 g, 0.1 mmol) was added to a flask

173   containing dry acetonitrile (10 mL) and reaction mixture was stirred for 7 h at 333 K and final

174   products was analysed by the UV spectra and one of the reaction product benzophenone is

175   confirmed by LC-MS analysis.

176   **2.9.1 Photocatalytic degradation of the RhB under the UV and visible light irradiations.**

177   The photo catalytic activities of the FC and ZEMC were evaluated in degradation of the

178   RhB under UV as well as visible/ H$_2$O$_2$ (1mmol) in a cylindrical glass reactor diameter 66 X 98

179   mm with contains a water jacket at room temperature. The mercury (Hg) (100W, 365 nm) was

180   used as UV light source and a 250 W tungsten lamp (Philips) used as a visible light source

181   equipped with UV cut-off filter were used to trigger the photo decomposition reactions. The

182   catalysts 0.06 mmol M(II)L.2ClO4 (0.05 g in case of ZEMC) was added to 0.01 mmol of 100

183   mL RhB aqueous solution and the above catalysts were added separately for the both

184   UV(visible/H_2O_2) irradiations. After optimising the reaction conditions in dark at room

185   temperature the suspension was irradiated by light sources. The 3 mL of the solution was

186   collected for each predetermined time intervals (30 min) and consequence spectral changes

187   were monitored by UV–Vis spectra using a Perkin Elmer Lambda 35 spectrophotometer

188   operating in the range 200-800 nm at 554 (± 1) nm for 3 h. The percentage of the conversion

189   and reaction rates in photo degradation process was formulated by the Lambert-beers

190   correlation formulae

191   $$A = \varepsilon.c.l \tag{1}$$

192   Here ε =molar extinction coefficient [M^{-1} cm^{-1}]. c= sample concentration =path length of

193   cuvette (1 cm).

194   **3.0 Results and discussion**

195   **3.1 Chemical and magnetic studies**

196   The chemical analysis (AAS) results are given in the Table: A (ESI †). The parent

197   zeolite unit cell formula $Na_{52}[(AlO_2)_{52}(SiO_2)_{140})]$ and Si/Al= ~2.7. The Silica aluminium ratio

198   (SAR) quite same in all exchange process. The consistency of the SAR suggesting the no

199   leaching of the aluminium during exchange processes and incomplete exchange of the sodium

200   metal ion with both copper (II) and nickel (II) also found. The gradually decrease in percentage

201   of the metal from free exchange metal to and metal ligand exchanged zeolite (ZEMC). shows

202   the formation and presence of the Schiff base metal hydrazone complexes in the cavity of

203   zeolite. The AAS analysis, SEM/TEM(EDAX) and XPS analysis confirms the presence of

204 the, nickel (II), copper (II), Si and Al. The simple gouy balance technique was used for the

205 magnetic susceptibility studies. This revels the magnetic moment value at 1.78 BM for the

206 Cu(II)L.2ClO$_4$ this value slightly change to 1.92 BM for Cu(II)L-Y. The nickel (II) complex

207 has shown the diamagnetic nature. These values well matched with the earlier reports for the

208 mono nuclear complexes.[14]

209 **3.2 Infrared Spectroscopy (FTIR)**

210 The FTIR spectra of H$_2$L, NaY, Ni(II)L.2ClO$_4$, Cu(II).2ClO$_4$, Ni(II)-Y and Cu(II)-Y are

211 provided in ESI† (Fig. S7 - S12). The shifts in bands, their peak assignments in wavenumber

212 are listed in the Table 1. The Fig. S7 shows the disappearance of the aldehyde carbonyl band.

213 The bands in the FTIR spectra of ligand H$_2$L and the appearance of three new bands at 1618

214 cm^{-1}, 1603 cm^{-1} and 1660 cm^{-1} due to the stretching frequency of -C=N, C=N (π) and -C=O

215 groups, respectively.[15,16]. This clearly indicates that the primary amino group of the isoniazid

216 was involved in the formation of azomethine group in the Schiff base ligand. The FTIR spectra

217 of the Ni(II)L.2ClO$_4$ and Cu(II)L.2ClO$_4$ (ESI† (Fig. S7& S8) appear a band in the region of

218 1505-1520 cm^{-1} assigned to valence vibrations of v(O-C=N) due to the enolization of H$_2$L

219 during complexation.[17] The vibrations of the C=O group at 1660 cm^{-1} is disappeared for the

220 complexes and also a new broadband appears at 1135-1150 cm^{-1} assigned to enol form of

221 deprotonated hydrazone (v$_{C-O}$).[18] . The azomethine (N=C) group frequencies appeared at the

222 lower region (1594-1585 cm^{-1}) when compared with the ligand frequency 1618 cm^{-1} due to the

223 metal ion coordination.[19]. This observation indicates the M(II) ion coordinate with the dianionic

224 tetradentate N$_2$O$_2$ chelating ligand of the azomethine nitrogens and enolic oxygens. Moreover

225 bands corresponding to one of the N-H groups also disappear and new medium bands appear

226 around 1020 cm^{-1} which corresponding to the N-N frequency. The pyridine (N=C) group

227 stretching frequency around 1603 cm^{-1} remains same in all complexes which shows metal ions

228 do not involve in the coordination with pyridine nitrogen. The bands around 1378 and 767 cm^{-1}

229　are due to the bending vibrations of C-H of the aromatic ring. At lower frequency region the

230　complexes exhibit medium intensity bands around 414-490 cm^{-1} and 518-580 cm^{-1}

231　corresponding to M-N and M-O vibration modes respectively. From the ESI† (Fig. S8 & S9) a

232　broad signal was appeared in the region of 1114 and 1084 cm^{-1} due to the antisymmetric

233　stretching vibration of the perchlorate ions in complexes and a medium band at about 628 cm^{-1}

234　and 1000 cm^{-1} due to the antisymmetric bending and stretching vibrations of the metal

235　coordinated perchlorate moiety are confirmed.[20].

236　　　The FTIR spectral data can give the information of crystallinity of zeolite and

237　encapsulation of complexes. The FTIR studies of NaY ESI† (Fig. S10) and ZEMC (Fig. S11 &

238　S12) show that the peak intensities are weak due to the low concentration of the complexes in

239　the cavity of zeolite. The NaY bands in the range 3600-3200 cm^{-1} due to the adsorbing

240　tendency of the surface hydroxyl groups and the bands at 1200-450 cm^{-1} are due to the lattice

241　(Si/Al)O$_4$ vibrations.[21.] The bands of ZEMC and FC are exhibit bands in this region of 1615-

242　1200 cm^{-1} which was absent in the NaY. The azomethine -C=N group stretching frequency is

243　observed around 1595 cm^{-1} and the pyridine -N=C group stretching frequency is observed as

244　broad band around 1616 cm^{-1} due to bending frequency of -OH groups the ZEMC. The C-O

245　and N-N stretching frequencies were merged with the O-Si-O and O-Al-O lattice vibrations and

246　all other peaks which were corresponding to C-H, C-C, C=C band vibrations of ZEMC are

247　almost similar to FC. This observation confirms not only presence of metal complex in zeolite,

248　but also no change in the lattice nature of zeolite. All ZEMC was shown peaks around 1121,

249　1020, 790 and 710 cm^{-1} because of the zeolite.[22] indicating not only no consequent changes in

250　the zeolite cavities but also no de-alumination during the encapsulation process. The new fairly

251　less intense bands appearing at the lower frequency region around 550 cm^{-1} and 430 cm^{-1} in the

252　encapsulated complexes originate from M-O and M-N vibrations.[23]. These observations suggest

253　that very weak involvement in the metal ion in coordination in the zeolite. The FTIR spectral

254   analysis provided the evidence for the encapsulation of metal complexes in the zeolite matrix

255   and crystallinity of the host zeolite.

256   **Table.1: FTIR spectral values in cm^{-1} for the FC and ZEMC.**

Sample	$\nu_{(C=O)}$	$\nu_{(C=N)}$	$\nu_{(C=N-N=C)}$	$\nu_{(C-O^-)}$	$\nu_{(C-O-C)}$	$\nu_{(N-N)}$	$\nu_{(N-H)}$	$\nu_{(M-O)}$	$\nu_{(M-N)}$
			Wave number	(cm^{-1})					
SAL	1706	-	-	-	1230, 1307	-	-	-	-
H$_2$L	1661	1603	1618	-	1242, 1302	961	3034	-	-
Ni(II)L	-	1602	1583,1504	1147	1244, 1301	1024	-	582	444
Cu(II)L	-	1605	1575,1512	1152	1245, 1293	1020	-	540	492
Ni(II)L-Y	-	1612	1598,1518	1155	1245, 1306	952-1000	-	530	430
Cu(II)L-Y	-	1615	1554,1506	1167	1268, 1315	947-1000	-	579	463

257

258   3.3 Optical absorption spectra /DRS studies

259   The UV-visible spectra were recorded for H$_2$L, FC and ZEMC and the corresponding

260   spectra are given in the Fig.1 (a-e). The absorption spectrum of the H$_2$L in UV region exhibits

261   three absorption bands at 272 nm ($\pi\rightarrow\pi^*$), 288 nm ($\pi\rightarrow\pi^*$), and 332 nm (n$\rightarrow\pi^*$).

262   Ni(II)L.2ClO$_4$ exhibit absorption bands at 258 nm and 352 nm due to the intra ligand $\pi\rightarrow\pi^*$

263   transitions and n$\rightarrow\pi^*$ transitions of azomethine(C=N) groups respectively. It shows a broad

264   visible band centred at 650 nm assigned to $^1A_{1g}$ to $^1B_{1g}$ transitions.[24] In addition the electronic

265   spectral values in this region might be suggested slight distortion of the square planar

266   geometry. The Ni(II) might have surrounded with the two imino nitrogen and two enolic form

267   oxygen atoms.[25] The Cu(II)L.2ClO$_4$ in DMSO & methanol also exhibits the bands at 268 nm

268   and 348 nm due to $\pi\rightarrow\pi^*$ and n$\rightarrow\pi^*$ transitions respectively. The square-planar Cu(II) complex

269   gives a broad absorption band between 600 to 700 nm by Jahn-Teller distortion. Due to the

270   N$_2$O$_2$ moiety, the geometry of the copper complex might be distorted from octahedral to

271   tetragonal or planar geometry.[26]

272   The DRS spectra of the ZEMC are shown in Fig.1 (d&e). Ni(II)L-Y shows three

273   characteristic bands at 223-269 and 334 nm due to the $\pi \to \pi^*$ and $n \to \pi^*$ transitions,

274   respectively and a broad band centred at 608 nm for the d-d transitions. Cu(II)L-Y also shows

275   the corresponding peak values at 222-266 nm and 325 nm are assigned to $\pi \to \pi^*$ and $n \to \pi^*$

276   transitions respectively. The Cu(II)L-Y shows a broad peak at 650 nm due to d-d transition.[27,28]

277   The comparison of the ZEMC with FC the peaks shift was inidicates the electronic transitions

278   associated influence of the zeolite matrix and elongated axial coordination of the complexes.

279   This further gives an idea about all complexes do not undergo a similar kind of structural

280   change in zeolite-Y and (Si/Al)O$_4$ groups might be influence a peak shift. However, the

281   presence of the similarly electronic transitions in the ZEMC in comparison to the neat complex

282   (FC) in solution gives one of the probability to formation of geometry and stability of the

283   complexes inside cavites of the zeolite-Y.
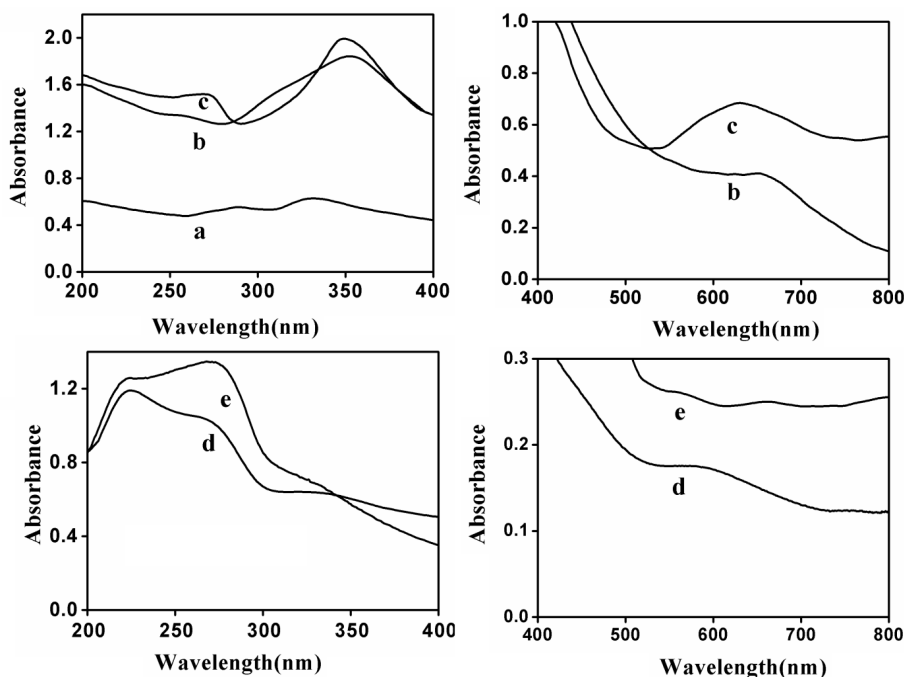
Fig.1: UV-VIS/DRS of the (a)H$_2$L, (b) Ni(II)L.2ClO$_4$ (c) Cu(II)L.2ClO$_4$ (d)Ni(II)L-Y and (e) Cu(II)L-Y

297

298   **3.4 EPR spectral studies**

299   The EPR spectra of Cu(II)L.2ClO$_4$ and Cu(II)L-Y in liquid nitrogen temperature were

300   recorded and presented in Fig.2 (a & b**).** The g values are calculated relative to

301   tetracyanoethylene g-marker (TCNE, g=2.0023.). The copper (II) (I=3/2) complex is typically

302   anisotropic in nature at LNT. Nitrogen hyperfine splitting can be clearly seen in the spectrum.

303   The Cu(II)L.2ClO$_4$ shows values of g$_\parallel$, g$_\perp$ and g$_{av}$ at 2.34, 2.079 and 2.16 respectively. The g$_\parallel$ >

304   g$_\perp$ > 2.0023 indicates the covalent environment of the metal ion with the Schiff base and also

305   the A$_\parallel$ value at 148 T indicates the coordinating metal environment might have a square planar

306   geometry and unpaired electron in the dx^2-y^2 orbital. Further, Cu(II)L.2ClO$_4$ exhibit the G

307   value [G=(g$_\parallel$ - 2.0023)/ (g$_\perp$ - 2.0023)]= 4.56 is slightly greater than 4, which indicates that the

308   no exchange interaction in the (mono nuclear) copper(II) complex. It is evidenced that twist in

309   the geometry may have octhahedrally distorted square planar geometry or metal with incipient

310   axial coordination.[29,30] The Cu(II)L-Y also exhibit the g tensor values at g$_\parallel$ (2.29) > g$_\perp$ (2.09) >

311   g$_{av}$ (2.0023) this might be due to the hyper fine coupling of copper (II) with the tetradentate

312   N$_2$O$_2$ with axial planar symmetry and the peaks are well isolated with less intensity. The hyper

313   fine splitting factor (A$_\parallel$) at 160 T indicates presence of unpaired electron in the dx^2-y^2 orbital

314   with axial interaction leads to elongated tetragonal distorted octahedral geometry with the

315   square planar moiety.[31] The Cu(II)L-Y exhibits G value (G = (g$_\parallel$ - 2.0023)/ (g$_\perp$ - 2.0023)) are

316   slightly greater than 4 its indicates that no copper(II) ion exchange interaction. It has been

317   reported that high g$_\parallel$ values are common to the six coordinate Cu(II) complexes with ligand

318   containing hard donors such as nitrogen and oxygen. The A$_\parallel$ value of the Cu(II) L-Y is larger

319   than Cu(II)L.2ClO$_4$, this might be either electrostatic interaction of the sodium ion or due to

320   the silica skeleton. These observations conclude that geometry of the mono nuclear copper

321   complex in the free state and encapsulated sate almost same and electronic studies also supports

322   the EPR observation.[32]

323
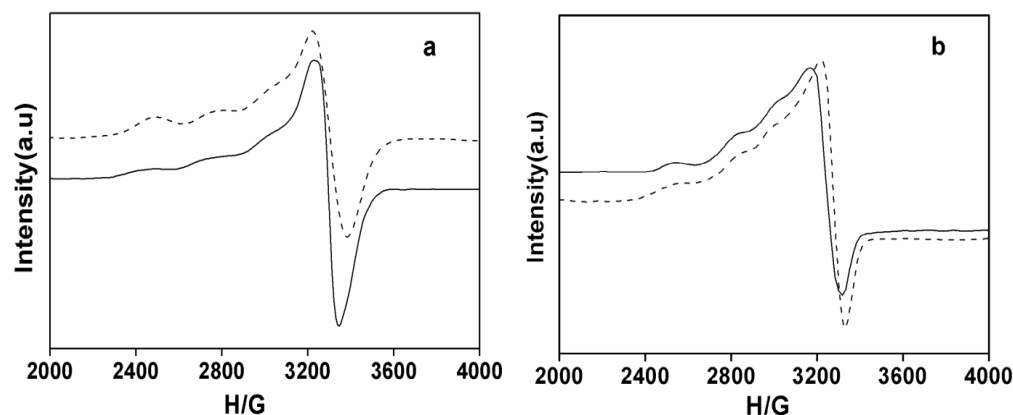
324   **Fig.2:** Experimental (thick) line stemming (dash) line spectra X-band epr spectra of the (a)

325     $Cu(II)L.2ClO_4$ (b) Cu(II)L-Y at LNT (the spectrometer settings microwave power frequency

326   9.43GHz: microwave power 13mW: modulation frequency KHz; modulation amplitude.2G)

327   **3.5 X-ray Photoelectron Spectroscopy analysis**

328   The XPS spectra of ZEMC and FC are given in the ESI† (Fig:S 13a-d) it reveals the

329   presence of the C, N, O, Na, Si, Al, Ni(II) and Cu(II) and which confirms respective surface

330   chemical state of the elements.[33] The peaks are related to carbon in free and encapsulated

331   complexes show highly intense broad bands. The C 1S, N 1S, O 1S and Cl 2P appear at 285.1,

332   400.0, 531.2 and 207 eV respectively[34]. From Fig.3(a-e) the C 1s XPS traces can be

333   deconvoluted into five peaks corresponding values 284.6 eV, 285.1 eV, 286.4eV and 288.8 eV

334   are attributed to the carbon sp^2 (C=C), carbon sp^3 (C-C), imine C=N, aryl ether (C-O-C) and

335   carbonyl (C=O), respectively. The C=O group binding energy 288.9 eV disappears for the

336   complexes and also a new broad peak appears at 286.9 eV assigned to enol form of

337   deprotonated hydrazone (C-O⁻) during complexation.[35]

338   The XPS studies of FC reveal the multiplicity of electon, valence state, magnetic states of

339   metal ions and stereochemical configurations. The phenomenon of shake-up satellite peaks in

340   the X-ray photoelectron spectra of 2p level spectra of the nickel(II)and copper(II) complexes

341   are well documented.[36.] The appearance of shake-up satellite lines behind the M(II) 2p core

342   lines of the Ni(II) and Cu(II) was shown covalency, magnetic and geometric properties of the

343   compound. These XPS results are matched with an earlier investigation.[37]. From Fig.4 and

344   Table 2 the traces of Ni(II)L.2ClO$_4$ indicate that no shake-up satellite peaks are observed

345   behind the region of 878 eV for the Ni(II)(2p) and hence it confirms the planar form and

346   diamagnetic nature of Ni(II).[38,39] In 2p level spectra of Ni(II)L-Y, the $\triangle$2P (ca.1.73 eV) more

347   when compared to Ni(II)L.2ClO$_4$. This may be due to existence of intracrystalline hydroxyl

348   groups and electrostatic interaction with (Si/Al)O$_4$ lattice.

349   From ESI† (Fig S 14c&d) The copper (II) complexes was shown shake up satellites where

350   as the diamagnetic Cu(I)(3d^{10}) never give any satellite peaks. Hence the Cu(II)L.2ClO$_4$ and

351   Cu(II)L-Y shows the paramagnetic nature(3d^9). This observations confirms the presence of

352   unpaired electron in dx^2-dy^2 orbital and EPR spectral data also supports the same.[40] The

353   broadening of Cu 2p$_{3/2}$ satellite peak was observed. It may be due to distortion of octahedral to

354   planar geometry. The Cu 2P peaks of Cu(II)L.2ClO$_4$ appears at the binding energy values at

355   934.12 eV and 953.87 eV as well as but the Cu(II)L-Y exhibits values at 934.90 eV, 954.30 eV

356   for 2p$_{3/2}$ and 2P $_{1/2}$ respectively. The Cu(II)L-Y also exhibits the same peak position similar to

357   Cu(II)L.2CLO$_4$ with the binding energy difference 0.41 eV. From FIG 4 the peak at 931.8 eV

358   represents the reduction of Cu(II) to Cu(I) this was caused by the X-ray irradiation during

359   acquisition time of the XPS analysis. But for nickel proximity the reduction is less, here xps

360   spectra observes the broadening of the 2p level peak observed.[41] The deconvoluted N1$_S$ and

361   O1$_S$ (ESI† Fig.S15 & 16) XPS traces shown the binding energy values also suggest that the

362   M(II) ion are coordinated with azomethine nitrogen and enol form of deprotonated oxygens in

363   both FC and ZEMC.

364   The NMR, ESI-mass and the above spectral studies confirm the possible proposed

365   structure of the complexes in the free and encapsulated systems as given in the **Scheme (A&B).**

366   **Table 2: Binding energy of the FC and ZEMC**

Compound	Binding energy (eV)						
	Si(2P)	Al(2P)	C(1S)	O(1S)	N(1S)	M(II) (2P)	△2P
Ni(II)L.2ClO$_4$	-	-	284.45	531.5	399.51	855.20, 873.13	17.45
Cu(II)L.2ClO$_4$	-	-	285.05	532.03	399.60	934.12, 953.87	19.03
Ni(II)L-Y	102.5	74.6	284.85	532.03	400.12	855.97, 875.10	19.02
Cu(II)L-Y	102.6	75.8	284.75	532.4	400.80	934.90, 954.30	19.35

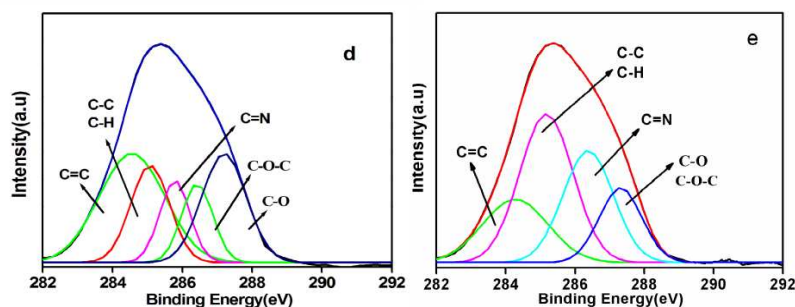**367**
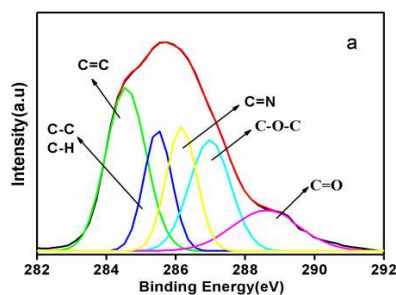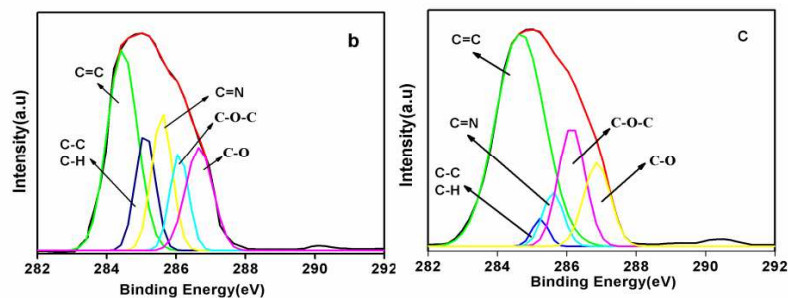
382   **Fig.3:** Deconvoluted XPS of the C1s region for (a) H2L, (b)Ni(II)L.2ClO4, (d)Cu(II)L.2ClO4,

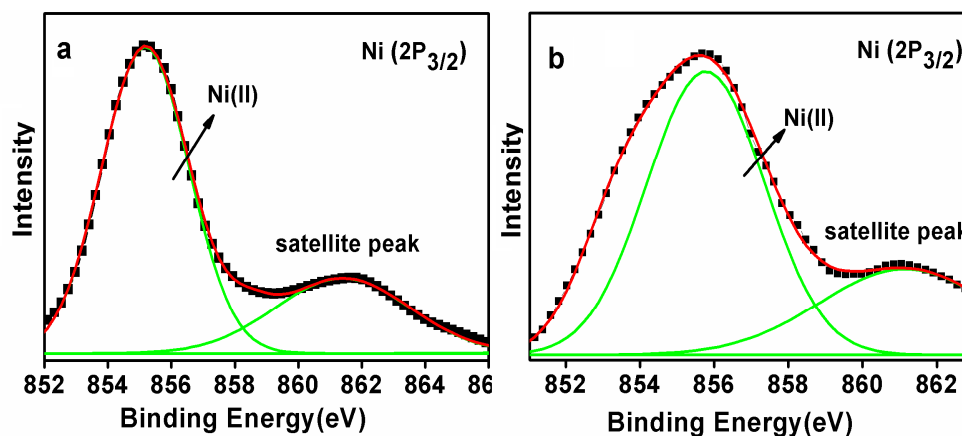**383**   (c)Ni(II)L-Y and (e) Cu(II)L-Y.
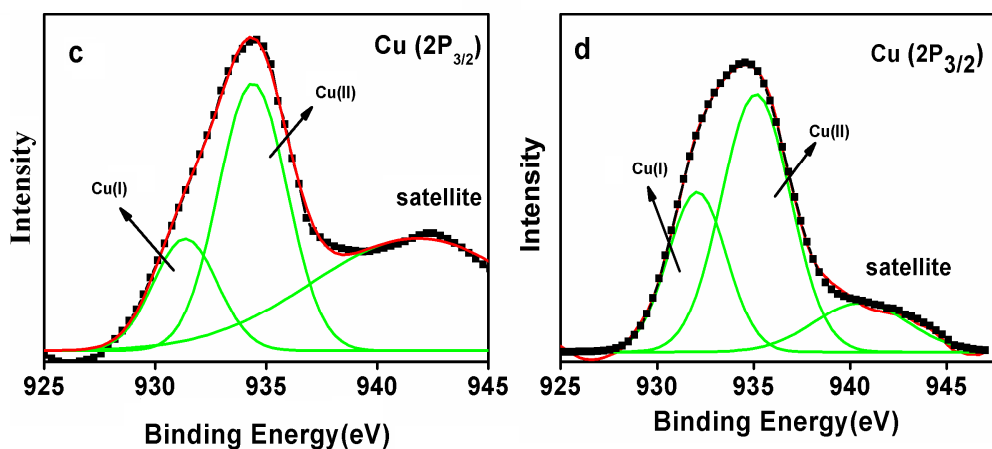
384

385

386

387

388

389

390

391

392

393

394

395

396

397

Fig.4: M(II)p$_{3/2}$ XPS patterns of the (a) Ni(II)L.2ClO$_4$ (b) Ni(II)L-Y (c) Cu(II)L.2ClO$_4$ and (d) Cu(II)L-Y.

3.6 Powder X-ray diffraction

The XRD of the NaY, Ni(II)L-Y, Cu(II)L-Y, NI(II)L.2ClO$_4$, and Cu(II)L.2ClO$_4$ were recorded at room temperature shown in Fig. 5(a-c). The XRD patterns of the Ni(II)L-Y, Cu(II)L-Y are compare with the of Na-Y, though minute change in the peak intensity was observed. The relative peak intensities of the 220, 311, and 331 reflections for ZEMC slightly decreased when compared with the parent zeolite reflections, it can be attributed change in sodium ion exchanged by metal moieties. The NaY has shown peak intensity I$_{331}$>I$_{220}$>I$_{311}$, but in case of the Ni(II)L-Y and Cu(II)L-Y the corresponding peak intensities I$_{331}$>I$_{311}$=I$_{220}$ and I$_{331}$>>I$_{311}$>I$_{220}$ are observed.[42] The Ni(II)L-Y shows three new peaks at 2θ values 12.9°, 27.1°

409 and 40.37° and Cu(II)L-Y also shows new peaks at 18.2°, and 42.6°.The new peak suggest

410 allocation and formation of the metal complexes in the cavity of zeolite. In another way FC

411 makes surface reduction of Na-Y during encapsulation process, hence peak intensity was

412 observed to low. (Asterisks fig 5).[43] The NaY crystalline nature does not change during the

413 impregnation.

414

415

416

417

418

419

420

421
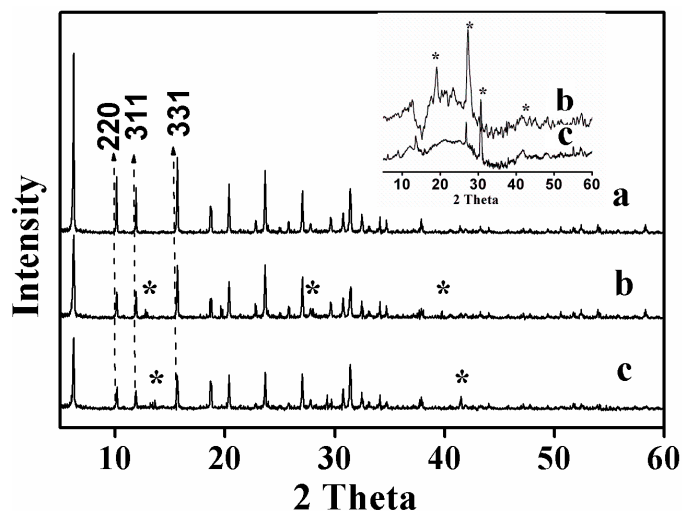
422 **Fig.5:** XRD spectra of (a)NaY, (b)Ni(II)L-Y and (c) Cu(II)L-Y (stick diagram shows XRD

423 patterns of the (b) Ni(II)L.2ClO$_4$ and (c) Cu(II)L.2ClO$_4$).(Asterisks indexes the presence of the

424 metal complexes on the cavity of the zeolite)

425 **3.7 BET analysis**

426 The Brunauer-Emmett-Teller (BET), N$_2$ adsorption/desorption isotherms, surface area

427 and the pore volume studies for the NaY, Ni(II)L-Y and Cu(II)L-Y was shown in the (ESI† Fig

428 S17a-c). The pore size distribution curves of samples was evaluated from adsorption branches

429 of the isotherms (stick diagrams) using the BJH method these composites had type IV

430 isotherms initially upto at p/p$_0$ =0.35 with a step increased at p/p$_0$ =0.35-0.7, reflecting their

431 narrow pore size distribution due to the capillary condensation of the pores i.e. presence of the

432 guest molecules in the pores of zeolite [44, 45] The surface area of zeolite was observed to be 600

433 m^2/g. But in case of ZEMC surface area was drastically reduced to 305 m^2/g and 230 m^2/g

434 respectively. The average pore size of free zeolite was 0.62 nm and it was reduced to 0.26, 0.17

435 nm on Ni(II), Cu(II) it may due to presence metal complexes in pores of zeolite. This clearly

436 suggesting the FC was encapsulated in the cavities of zeolite. The surface analysis revels the

437 ZEMC based on the metal loading, hence the copper (II) complexes was shown more reactive

438 sites than nickel (II).

439 **3.8 Thermal analysis**

440 The TG/DTG curves of FC and ZEMC were performed in static air atmosphere and

441 were shown in Fig 6(a-e). In the case of ZEMC the TG curve show a residual mass of around

442 85% clearly suggesting and shows thermal stability of composites. The DTG curves of FC and

443 ZEMC clearly shows the multi step decomposition. In case of Ni(II)L.2ClO$_4$, the first step

444 between 303- 423 K corresponds to the loss of coordinated counter ions with a mass loss of

445 8%. In the second step, the continuous loss of ligand molecules of the complex was observed in

446 the temperature range upto 731 K with a mass loss of 79%. The residual mass 12% corresponds

447 to the formation of nickel oxide. In the case of Cu(II)L.2ClO$_4$, the mass loss of (17%) lattice

448 water and perchlorate molecules occurs below 513 K. A further step corresponds to the

449 degradation of Cu(II)-ligand moiety between 523-773 K with a mass loss of 70%. The residual

450 mass 11% indicates the formation of CuO.[46] From the Fig (6 c&d) DTG analysis the peak

451 temperature of ZEMC was higher when compared with peak temperatures of the FC. This

452 clearly suggests the metal free complexes were strongly inclusion in the cavities of zeolite

453 From Fig(7e) the NaY weight loss(15%) take place sharply in one step due to the presence of

454 water molecules, when comparison of these observations also suggesting the presence of the

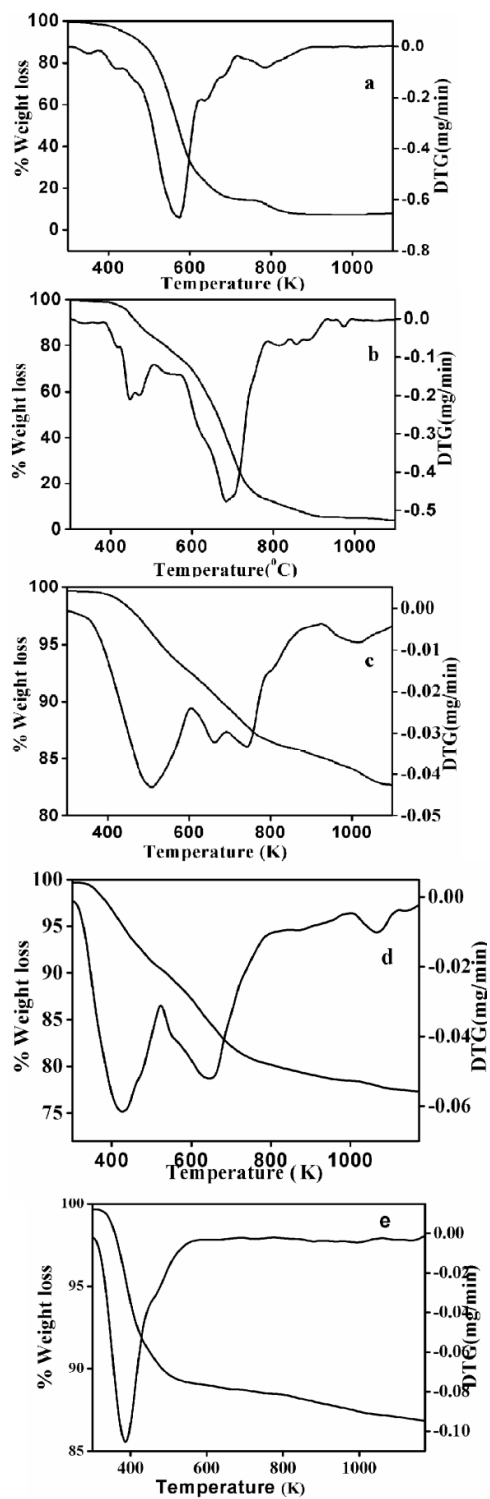455 metal complexes in the zeolite cavities.

456
457
458
459
460
461
462
463
464
465
466
467
468
469
470
471
472
473
474
475
476
477

478   **Fig. 6:** TG-DTG curves of the (a) Ni(II)L.2ClO$_4$ (b) Cu(II)L.2ClO$_4$ (c)Ni(II)L-Y, (d) Cu(II)L-Y

479   and (e) Na-Y.

480

481 **3.9: FESEM/HRTEM Analysis.**

482   Typical scanning electron micrographs obtained for the parent NaY and the ZEMC are

483 shown in Fig.7 (a-c). The, Na-Y possess shape of the particle is cubic angular. The SEM

484 analysis of the ZEMC shows crystal nature the Na-Y was remains almost same even after

485 complexation occurs in the cavities of the zeolite. From the (ESI† Fig: S18-21) EDAX spectra

486 of the ZEMC conclude the each elements present in the cavity of zeolite. SEM image elemental

487 mapping indicates that uniform distribution of elements in the cavities of zeolite. The elemental

488 mapping clearly suggests that the particle surface boundaries do not have surface complexes.

489 From image-J analysis software the histogram was plotted of the ZEMC. The average size of

490 the ZEMC particles is calculated by the based on the Gaussian fit of the size distribution

491 histogram NaY(ESI Fig: 25), Ni(II)L-Y and Cu(II)L-Y 98 nm corresponding average size are

492 around 145 nm, 165 nm and 180 nm respectively.[47,48]

493

494

495

496

497

498

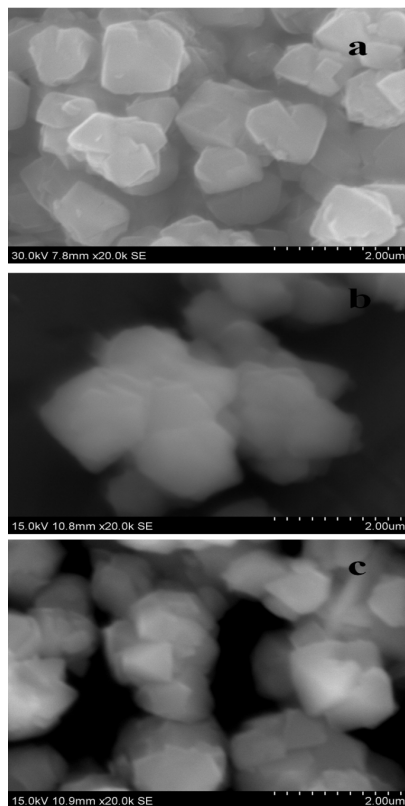**499**

500

501

502

503

504

505 **Fig.7:** The SEM image of the (a) NaY, (b) Ni(II)L-Y and (c) Ni(II)L-Y.

506   The TEM photographies of the parent NaY and ZEMC are shown in Fig.8 (a-c). This

507 reveals that structure of the solid supports was rectangular spheroid (tablet shape) and its

508 channels were well ordered. The encapsulated complexes Ni(II)L-Y and Cu(II)L-Y also show

509 opaque nature and well ordered shape but slight change in the surface edges and the negligible

510 agglomeration is observed when compared to parent zeolite. The morphology and the SAED

511 patterns of the Ni(II)L-Y and Cu(II)L-Y shows crystalline nature even after encapsulation of

512 the complex moiety in the cavities of zeolite.[48] The black dot present in the zeolite micrograph

513 itself hence if not indicating the surface present metal traces.
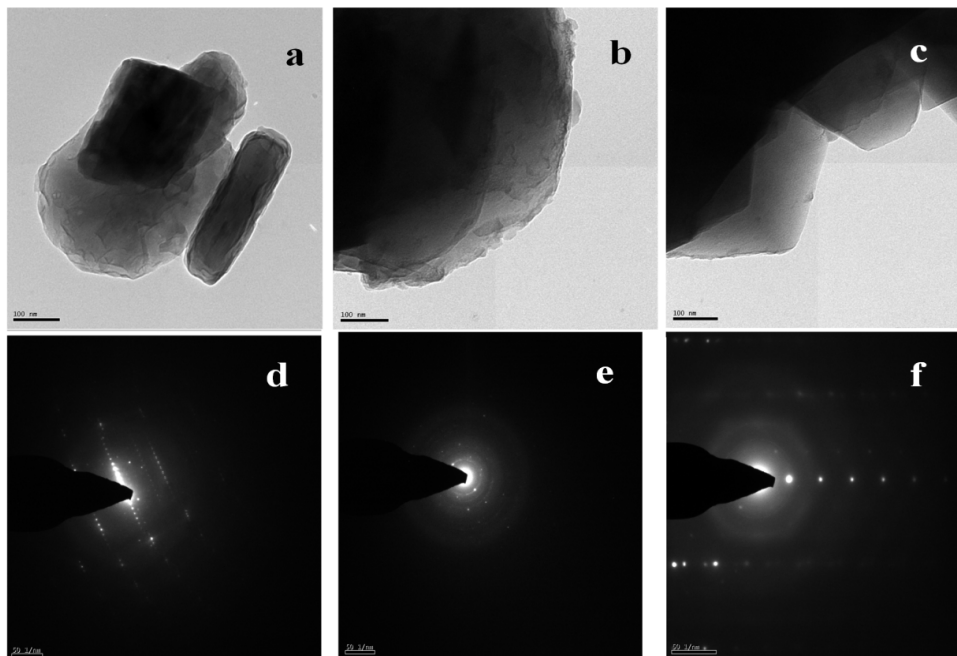
514

515

516

517

518

519

520

521

522

523

524

525

526 **Fig.8:** The HRTEM images of the (a) NaY, (b) Ni(II)L-Y and (c) Cu(II)L-Y and corresponding

527 SAED pattern (d) NaY, (e) Ni(II)L-Y and (f) Cu(II)L-Y

528

529

530

4 Catalytic studies

4.1 Interaction of the Ni(II)L.2ClO₄ and Cu(II)L.2ClO₄ with the hydrogen peroxide

The effect of hydrogen peroxide in the presence of the Ni(II)L.2ClO$_4$ and Cu(II)L.2ClO$_4$ was recorded with UV-VIS spectra shown in the (ESI † Fig: S 25a&b) with the 2:1 molar ratio of the H$_2$O$_2$ and metal complexes. The decrement optical density for the d-d transition peak value was observed and new peaks around 450 and 470 nm may indicate the existence of either metal activated oxygen radicals or the formation of the superoxo and oxodimer species during the homogeneous conditions at last it result a colour less solid particles. Same phenomenon may be expected for the ZEMC in the formation of the new intermediates adduct and it can improve the substrates rate of the reaction rate and selectivity. It was observed that the copper has hiegher tendency in formation of the reactive intermediates than nickel. ZEMC less probability to formation of the polymeric and dimerised oxo species along with metal (II) centres where as the free complexes shows this phenomenon. This assets may show and leads to improving the product formation in the liquid phase oxidation reactions.[49]

4.2 Catalytic activity and kinetic parameters of ZEMC and FC in BH oxidation.

The catalytic activity of the FC and ZEMC was studied in the liquid phase (mild) oxidation reaction of the BH, while using H$_2$O$_2$ is an oxidant. Generally the metal complexes oxidation reaction depends on formation of the perhydroxy and hydroxyl radicals in presence of the oxidants. The polymeric nature of the free complexes might show less activity even at H$_2$O$_2$. In absence of H$_2$O$_2$ BH oxidation was not occurred, so metal active center play crucial role in the BH oxidation. In presence of the FC the optimum conversion was observed with H$_2$O$_2$ due to formation the [M(II)(L)].H$_2$O$_2$ adduct as an intermediate. The adduct can be generate the perhydroxy(•OOH) •OH intermediates with Nickel (II) and copper (II). From section 4.1 the decrease in the peak intensity of charge transfer and d-d transitions of FC and

556 simultaneously formation of the radical intermediates was observed around 450 and 470 nm.[50]

557 The BH oxidation the spectral change and consequences of the absorption spectra recorded at

558 223 and 259 nm. The aliquot samples were collected from reaction mixture for every 60 min

559 and absorbance values were recorded at 223($\pm$2) nm. From (ESI† Fig: S26a-e) the progressive

560 decrement of absorption bands for every 60 min and those corresponding product

561 benzophenone peaks also been absorbed at 250 and 340 nm.[51]. From the Fig. 9 (a) the

562 percentage of conversion for NaY, Ni(II)L.2ClO4, Cu(II)L.2ClO4, Ni(II)L-Y and Cu(II)L-Y

563 are 18%, 56%, 96%, 65% and 85% respectively (no significance conversion was observed even

564 at 12 h). The copper complex was shown the higher conversion of percentage than nickel in

565 both FC and ZEMC. The copper has more tendencies in the formation of the hydroperoxy

566 intermediates with H_2O_2 in acetonitrile medium than nickel. The Cu(II) is 15-electron species

567 and participate actively in this electron back-donation process, hence it show higher catalytic

568 activity in comparison to the corresponding 16-electron Ni(II) complex. The kinetic parameters

569 in BH oxidation also follow the pattern of conversion percentage. From the Fig. 9 (b) The

570 kinetic plot between $\ln(C_t/C_o)$ Vs time and plots shown the negative slope and the reaction

571 follows the pseudo first order kinetics. All kinetic reactions show the same phenomenon. It may

572 be due to the usage of H_2O_2 and at constant BH concentration. The rate of the reaction follows

573 the first order rate .equation

574 $$\ln \left(\frac{C_t}{C_o}\right) = -k\,app.t \qquad (2)$$

575 Here C_t is the concentration of the BH at different time, C_0 is the initial concentration, t

576 is the time and k is the reaction rate constant in min^{-1}. From the figure 9 (b) The values of the

577 rate constant for NaY, Ni(II)L.2ClO$_4$, Cu(II)L.2ClO$_4$, Ni(II)L-Y and Cu(II)L-Y catalysts are

578 0.000375 min $^{-1}$, 0.00202 min $^{-1}$, 0.00491 min $^{-1}$, 0.00181 min $^{-1}$ and 0.00468 min $^{-1}$

579 respectively. The Cu(II)L-Y shows higher rate than Ni(II)L-Y this maybe formation adduct of

580 the per hydroxyl ion with copper (II) centres is more than nickel. The surface area of the

581   Cu(II)L-Y less with more active species even than large surface area catalysts.[52] Hence the

582   copper, nickel enhance the host-guest interaction, which leads to avoid the formation of

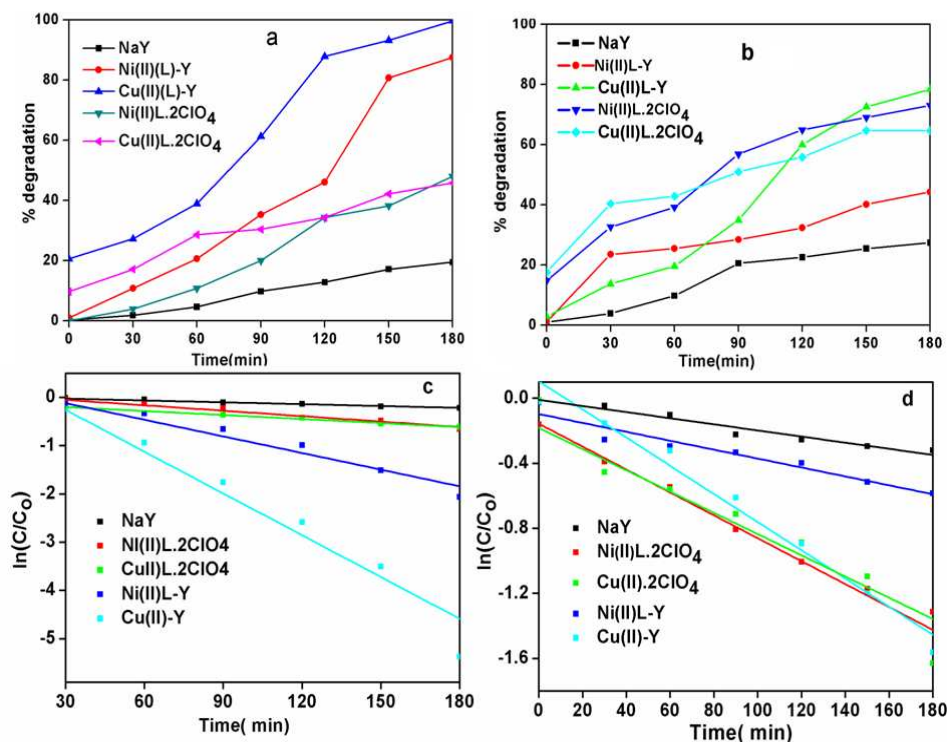583   polymeric metal species and. enhance the catalytic activity of the reaction.[53]

584

595

596   **Fig 9:** The graph (a) & (b) Time Vs % Conversion, (c) & (d) kinetic plots for the both FC and

597   ZEMC.

598   **4.3 Mechanistic issues for photochemical performance**

599   The photo catalytic degradation of the RhB with NaY, Ni(II)L-Y, Cu(II)L-Y,

600   Ni(II)L.2ClO$_4$ and Cu(II)L.2ClO$_4$ under UV/Visible irradiation has been studied. The

601   percentage of degradation and kinetic parameter calculated based Lambert-Beers law

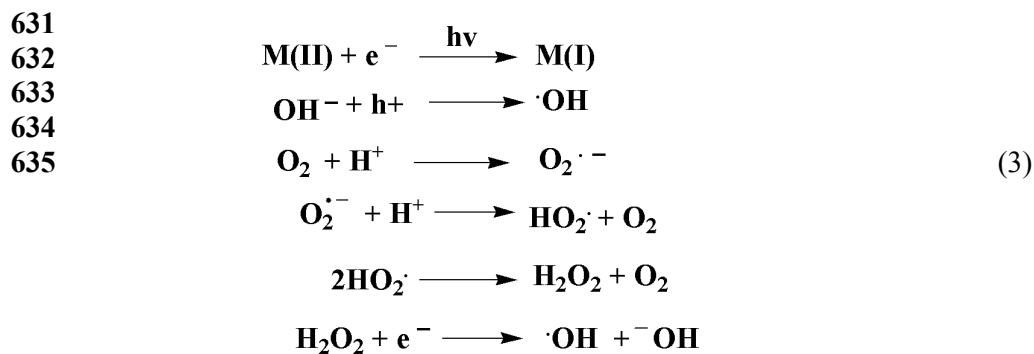602   (ε=103930 mol^{-1} cm^{-1} L) ($A = \varepsilon.c.l$)

603   The degradation efficiency was calculated by the optical absorption spectral analysis.

604   The aliquot samples of reaction medium were collected and the consequence absorption

605   changes were recorded at 554±1nm. The spectral changes were given in the ESI†. Fig S27 &

606   S28 The ZEMC has more degradation performance when compared to FC and NaY zeolite. In

607   both probe reactions the removal percentages are 15%, 88%, 100%, 55% and 50%(26%, 73%,

608   78%, 44% and 63% in case of visible light) for the NaY, Ni(II)L-Y, Cu(II)L-Y, Ni(II)L.2ClO$_4$

609   and Cu(II)L.2ClO$_4$ respectively. The metal enhance the acidity of zeolite during exchange

610   process, due to this photo catalytic performance, rate of reaction and removal efficiency of the

611   RhB also increases.[54] ZEMC could decrease the recombination of electron-hole pair and

612   enhance the photo catalytic performance. The apparent rate constant (k_{app}) and fixed

613   concentration of the H$_2$O$_2$ may leads to be concludes first order reaction. Fig. 9. reveals the

614   negative slope in the both cases. The rate constants for the both irradiations was NaY, Ni(II)L-

615   Y, Cu(II)L-Y, Ni(II)L.2ClO$_4$ and Cu(II)L.2ClO$_4$ (0.00128 min^{-1}, 0.375 min^{-1}, 0.0279 min^{-1},

616   0.0115 min^{-1} and 0.0285 min^{-1}(0.0018, 0.00653, 0.00704, 0.00274, 0.00866 min^{-1} in case

617   visible light). The ZEMC show higher activity because of it metal loading efficiency (from

618   tableA) which enhances the photo generated electron pairs (e- and h+). Photo generated holes

619   and electrons may react with surface hydroxyl groups are adsorbed water or O$_2$ to generate the

620   active oxidative ionic radical (O$_2^{\bullet-}$, $^-$OOH and •OH) from reaction medium. The O$_2^{\bullet-}$and $^\bullet$OH

621   radicals are very reactive and quickly oxidise organic species at the surface of the zeolite.

622   Hydroxyl radicals ($^\bullet$OH) is considered the most powerful oxidant (E^o = 2.8 V) amongst other

623   oxidants.[55] Even the acidic nature can enhance in the formation of the active radical limits the

624   degradation time. During the metal reduction from M(II) to M(I) the generation of the •OH

625   radical is more in presence of the H$_2$O$_2$[56]. Even the uniform distribution of metal in zeolite

626   cavity leads to fast photo generation of hydroxyl radical (equation 3). So the catalytic activity

627   depends on the percentage of metal, which results in more unsaturated surface coordination

628   sites.

629

630

631
632
633
634
635

$$M(II) + e^- \xrightarrow{hv} M(I)$$

$$OH^- + h+ \longrightarrow {}^{\cdot}OH$$

$$O_2 + H^+ \longrightarrow O_2^{\cdot -} \tag{3}$$

$$O_2^{\cdot -} + H^+ \longrightarrow HO_2^{\cdot} + O_2$$

$$2HO_2^{\cdot} \longrightarrow H_2O_2 + O_2$$

$$H_2O_2 + e^- \longrightarrow {}^{\cdot}OH + {}^-OH$$

636
637

638   From the ESI† Fig :S28 lower in the wavelength around 5 nm due to either the electrostatic

639   interactions with hydroxyl groups or formation de-ethylated spices of the dye molecule during

640   the degradation.[57] The photo generated electrons give more efficiency towards the hole

641   formation and minimize the band gap energy, mean while the formation of the ${}^{\cdot}OH$, ${}^{+\cdot}O_2H$, ${}^-O_2$

642   radical is a powerful oxidant and starts a cascade of oxidation reactions that can convert the

643   organic matter in solution completely into water, carbon dioxide and inorganic compounds[58, 59].

644   From (ESI† Figs:S38) the change in hypsochromic shift was around 25 nm, this cause the

645   detachments of chromophoric group present in the dye molecule and formation de-ethylated

646   intermediates of RhB molecules.[60]

647   **4.4 Recycle tests and metal leaching tests and catalytic activity**

648   The stable $(Si/Al)O_4$ moiety of zeolite does not allows the metal ion leaching. Due to the

649   higher cross sectional area of RhB, it is not possible to enter into the cavities of zeolite. While

650   using H_2O_2 the negligible metal leaching was observed. The approximate cross sectional area

651   the metal hydrazones complexes is 162 A^{o2} & 164 A^{o2} (measured by the chem sketch software

652   tool). It can be fit for the zeolite unit cell dimensions and in liquid phase encapsulation the free

653   complexes formation. Hence FC can be impregnates in the cavity of zeolite and stabilised by
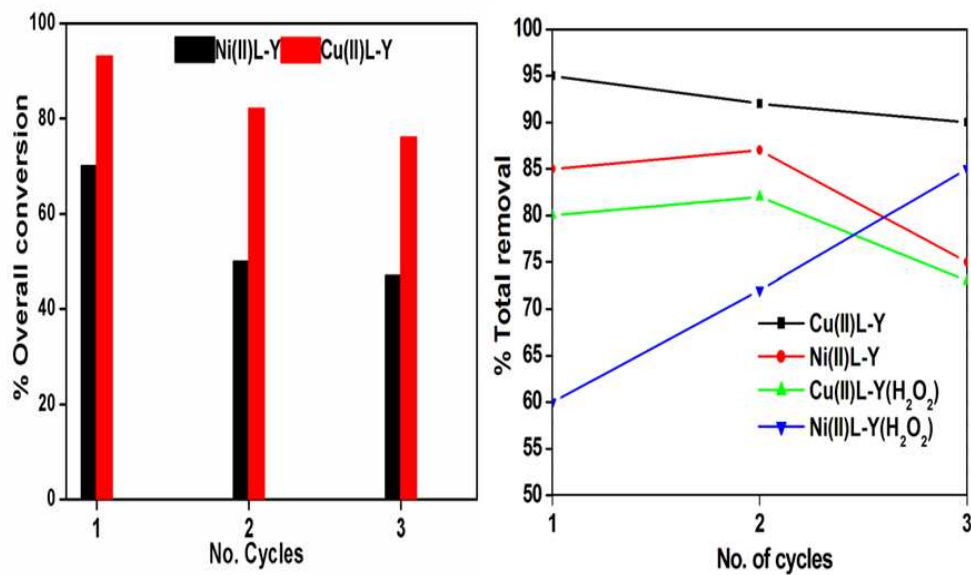
654

655

656

657

658

659

660

661

662

663

Fig 10:The recovered ZEMC overall percentage of conversion of BH oxidation(bar diagram)
and dye degradation(line diagram) in the three cycles.

(Si/Al)O$_4$ moieties. So, the metal ion leaching is very difficult after impregnation TBALE A..
After completing the reaction, ZEMC was recovered by nano-filtration and washed with water,
dilute HCl, acetonitrile and methanol mixture. The resulted colour solid was dried at 353 K for
6 h and each composite catalytic activity checked and the overall percentage provided in the
Fig. 10.

5. Conclusion

The Ni(II) and Cu(II) complexes of the H$_2$L and their complexes encapsulated in the
cavities of zeolite-Y were synthesized by FLM. The synthesized composite materials formation
and geometry within the zeolite matrix have been studied along with their free complexes by
several spectroscopic, thermal analysis, sorption and microscopic techniques. In both probe
reactions the FC(ZEMC0 mild oxidation of the BH and photo catalytic degradation
performance of were studied. From these studies the catalytic performance depends on the not

679   only surface area but also percentage of the metal present in cavities of the zeolite. The

680   generation of the perhydroxyl and hydroxy radical intermediates adduct(M- OOOH) teh

681   influence rate of conversion percentage. The optical spectral data and LC-MS data has shown

682   the benzophenone fragments in the BH oxidation. Photocatalytic reaction the removal

683   percentage of the dye also depends $^{\bullet}OH$, $^{+\bullet}O_2H$, $^{-}O_2$ radical is a powerful oxidant and starts a

684   cascade of oxidation reactions that can convert the organic matter in solution completely into

685   water, carbon dioxide, and inorganic compounds. In the dye removal and BH oxidation the

686   apparent rate conatant(k_{app}) if representation the pseudo first order reaction in all cases. here the

687   percentage of the conversion if more for the copper complexes than nickel. Hence the surface

688   active species accelerate the rate of the reaction in both cases. The surface area and percentage

689   of the copper (Table:A ESI†) might influence the rate of the reaction rather than average

690   particle size and crystalline nature.

691   **Acknowledgements**

697   **Appendix A. Supplementary data†**

698   ^{1}H and ^{13}C-NMR spectra, ESI-mass, FTIR, N1s, and O1s deconvoluted XPS spectral

699   trace with survey graph and M(II) 2p spectrum. N_2 isotherms, UV-VIS Spectral change,

700   microscopic analysis, percentage of the nickel, copper, silica and aluminium, The recovered

701   catalysts DRS/ UV-VIS spectra, PXRD and LC-MS are given in the electronic supplementary

702   data.

703

704 **References**

705 1 P. Games, P. G. Aube, W. L. Driessen and J. Reedijk, *Chem. Soc. Rev.,* 2001, **30**, 376.

706 2 M. L. Marin, L. S. Juanes, A. Arques, A. M. Amat and M. A. Miranda, *Chem. Rev.,* 2012,

707   **112**, 1710.

708 3 J. M. Bregeault, *Dalton Trans.,* 2003, **17**, 3289.

709 4 D. Habibi, A. R. Faraji, M. Arshadi and J. L. G. Fierro, *J. Mol. Catal. A: Chem.,* 2013, **372**,

710   90.

711 5 J. Jiang, R. B. Rao and Z. Hu, *Chem. Soc. Rev.,* 2011, **40**, 3599.

712 6 B. Agboola, K. Ozoemena and T. Nyokong, *J. Mol. Catal A: Chem.*, 2005, **227**, 209.

713 7 D. J. Xuereb and R. Raja, *Catal. Sci. Technol.*, 2011, **1**, 517.

714 8 A. C. Pradhan, B. Nanda, K. M. Parida and M. Das, *Dalton Trans.*, 2013, **42**, 558.

715 9 X. J. Hong, X. Liu, J. B. Zhang, X. Wu C. L. Lin, Y. J. Ou, J. Yang, H. G. Jin, and Y. P.

716   Cai,   Cryst Eng Comm**., accepted manuscript.** DOI: 10.1039/C4CE01207K.

717 10 10. A. H. Ahmed and M. S. Thabet, *J. Mol. Struct.*, 2011, **1006**, 527.

718 11 L. Maryam, R. Saeed, D. Derakhshan and Zeinab, *Chin. J. Chem.*, 2011, **29**, 2439.

719 12 B. Neppolian, H. C. Choi, S. Sakthivel, B. Arabindoo and V. Murugesan, *J. Hazard.*

720   *Mater.*, 2002, **89**, 303.

721 13 C. N. Reddy, K. Suman, K.P. Sai, S. Thennarasu, A. B. Mandal, *Dyes and Pigments*., 2012,

722   **95**, 606.

723 14 F. Brezina, H. Tillmannova, and Z. Sindelar, *Chem. Papers.*, 1986, **40**, 727.

724 15 L. R. Martins, E. T. Souza, T. L. Fernandez, B. De Souza, S. Rachinski, C. B. Pinheiro, R.

725   B. Faria, A. Casellato, S. P. Machado, A. S. Mangrich and M. Scarpellini, *J. Braz. Chem.*

726   *Soc.*, 2010, **21**, 1218.

727 16 P. V. Bernhardt, L. M. Caldwell, T. B Chaston, P. Chin and D. R. Richardson, *J. Biol.*

728   *Inorg Chem.*, 2003, **8**, 866.

729   17 A. Cukurovali, I. Yalmaz and S. Kirbag, *Trans. Met. Chem.*, 2006, **31**, 207.

730   18 S. Sujatha, S. Balasubramanian, H. K. Fun and K. Chinnakali, *Polyhedron.*, 2008, **27**, 1925.

731   19 M. R. Maurya, S. J. J. Titinchi and S. Chand, *J. Mol. Catal A: Chem.*, 2003, **201**, 119.

732   20 L. L. Sheu, H. Knozinger and W. M. H. Sachtler, *J. Molecular Catal.,* 1989, **57**, 61

733   21 S. M. Emam, F. A. E.Saied, S. A. E. Enein and H. A. E. Shater, *Spectrochim. Acta, Part A.*,

734   2009, 72, 291.

735   22 M. S. Niasari, F. Davar and K. Saberyan, *Polyhedron.*, 2010, **29**, 2149.

736   23 M. S. Niasari and A. Sobhani, *J. Mol. Catal. A: Chem.*, 2008, **285**, 58.

737   24 A. B. P. Lever. *Inorganic electronic spectroscopy*, Amsterdam, Netherland, Elsevier. 1984.

738   25 S. Yadav, M. Ahmad and K. S. Siddiqi, *Spectrochim. Acta, Part A.*, 2012, **98**, 240.

739   26 M. M. A. Neaimi and M. M. A. Khuder, *Spectrochim. Acta, Part A.,* 2013, **105**, 365.

740   27 M. V. Angelusiu, G. L. Almsjan, D. C. Ilies, T. Rou and M. Negoiu. *Chem. Bull.*

741   *Politehnica.*, 2008, **53**, 1.

742   28 V. P. Singh, A. Katiyar and S. Singh, *Biometals.*, 2008, **21**, 491.

743   29 S. Sujatha, S. Balasubramanian and B. Varghese, *Polyhedron.*, 2009, **28**, 3723.

744   30 S. Biswas, A. Dutta, M. Debnath, M. Dolai and K. K. Dasand, *Dalton Trans.*, 2013, **42**,

745   13210.

746   31 Y. Traa, D. M. Murphy, R. D. Farley and G. J. Hutchings, *Phys. Chem. Chem. Phys.*, 2001,

747   **3**, 1073.

748   32 S. Chandra, and X. Sangeetika, *Spectrochim. Acta, Part A.*, 2004, **60**, 147.

749   33 A. Godelitsas, D. Charistos, A. Tsipis, C. Tsipis, A. Filippidis, T. Manos, and D. Siapkas

750   *Chem. Eur. J.,* 2001, **7**, 3703.

751   34 A. R. Silva, M. Martins, M. M. A. Freitas, A. Valente, C. Freire and B. D. Castro, J. L. F.

752   *Microporous and Mesoporous Mater.*, 2002, **55**, 275.

753   35   R. Ferreira, C. Freire, B. Castro, A. P. Carvalho, J. Pires, and M. B. D. Carvalho, *Eur. J.*

754   *Inorg. Chem.*, 2002, **11**, 3032.

755   36   J. G. Dillard and L. T. Taylor, J. Electron. *Spectrosc. Relat. Phenom.*, 1974, **3**, 455.

756   37   J. Kawai, S. T. Suboyama, K. Ishizu, K. M. Amura, and M. Saburi, *Anal. Sci.*, 1994, **10**,

757   853.

758   38   A. M. Brisk and A. D. Baker, *J. Electron. Spectrosc. Relat. Phenom.*, 1975, **7**, 197.

759   39   L. J. Matienzo, W. E. Swartz Jr. S. O. Grim, *Inorg. Nucl. Chem. Letters*, 1972, **8**, 1085.

760   40   M. Fujiwarat, A. Matsushita and S. Ikeda, *Anal. Sci.*, 1993, **9**, 289.

761   41   K. K. Bania and R. C. Deka, *J. Phys. Chem. C.*, 2013, **117**, 11663.

762   42   M. S. Niasari, *Inorg. Chim. Acta.*, 2009, **362**, 3738.

763   43   K. O. Xavier, J. Chacko and K. K. M. Yusuff, *Appl. Catal. A: General.*, 2004, **258**, 251.

764   44   M. S. Niasari and A. Sobhani, *J. Mol. Catal. A: Chem.*, 2008, **285**, 58.

765   45   M. R. Maurya, A. K. Chandrakar and S. Chand, J. *Mol. Catal. A: Chem.*, 2007, **263**, 227.

766   46   R. M. Issa, S. A. Amer, I. A. Mansour and A. I. A. Monsef, *J. Therm. Anal. Calorim.,* 2007,

767   **90**, 261.

768   47   M. Jafrian, M. R. Avei, M. Khakali, F. Gobal, S. Rayti, and M. G. Mahjani, *J. Phy. Chem*

769   *C.*, 2012, **116**, 18518.

770   48   A. M. Fonseca, S. Gonc, A. P. Parpot and I. C. Neves, *Phys. Chem. Chem. Phys.*, 2009, **11**,

771   6308.

772   49   S. Biswas, A. Dutta, M. Debnath, M. Dolai and K. K. Dasand, *Dalton Trans.*, 2013, **42**,

773   13210.

774   50   W. Adam, W. Malisch, K. J. Roschmann, C. R. S. Moller and W. A. Schenk, *J. Organomet.*

775   *Chem.*, 2002, **661**, 3.

776   51   O. S. Mohamed, A. E. Aal, M. Gaber and A. A. Wahab, *J. Photochem. Photobiol. A:*

777   *Chemistry.*, 2002, **148**, 205.

778   52 C. Teixeira, P. Pescarmona, M. A. Carvalho, A. M. Fonseca and I. C. Neves, *New J. Chem.*,

779   2008, **32**, 2263–2269.

780   53 A. Jia, L. L. Lou, C. Zhang, Y. Zhang and S. Liu, *J. Mol. Catal. A: Chem.*, 2009, **306**, 123.

781   54 A. C. Pradhan, K. M. Parida and B. Nanda, *Dalton Trans.*, 2011, **40**, 7348.

782   55 P. Ciesla, P. Kocot, P. Mytych and Z. Stasicka, *J. Mol. Catal. A: Chem.*, 2004, **224**, 17.

783   56 M. Yin, Z. Li, J. Kou, and Z. Zou, *Environ. Sci. Technol.*, 2009, **43**, 8361.

784   57 X. Xue, K. Hanna and N. Deng, *J. Hazard. Mater.*, 2009, **166**, 407.

785   58 X. Zhou, X. Cui, H. Chen, Y. Zhu, Y. Song and J. Shi, *Dalton Trans.*, 2013, **42**, 890.

786   59 F. Chen, J. Zhao, and H. Hidaka, *Int. J. Photoenergy.*, 2003, **5**, 209.

787   60 H. Fu, C. Pan, W. Yao, and Y. Zhu, *J. Phys. Chem. B.*, 2005, **109**, 22432.

788

789   .

790

791

792

793

794

795

796

797

798

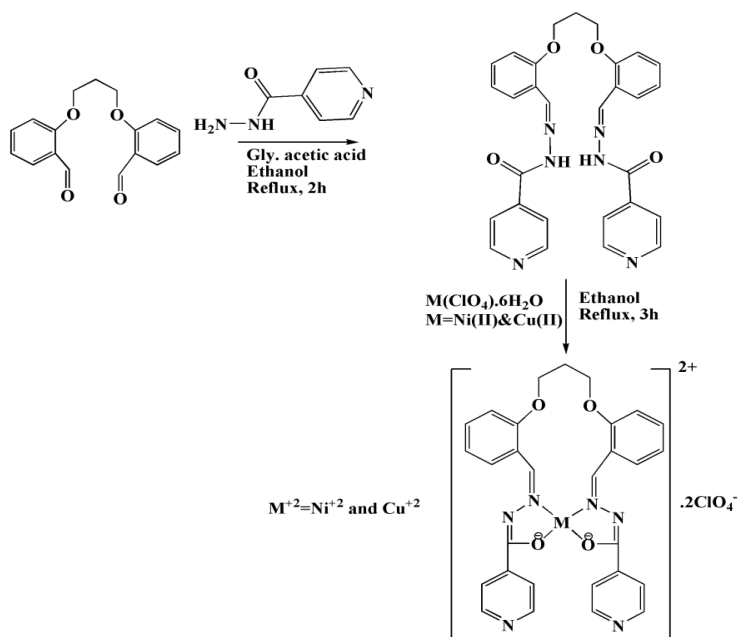799

800

801

802

803

804

805

806

807

808

809

810

811

812

813

814

815

816   **Scheme (A): The proposed reaction mechanism of Ni(II) and Cu(II) complexes**

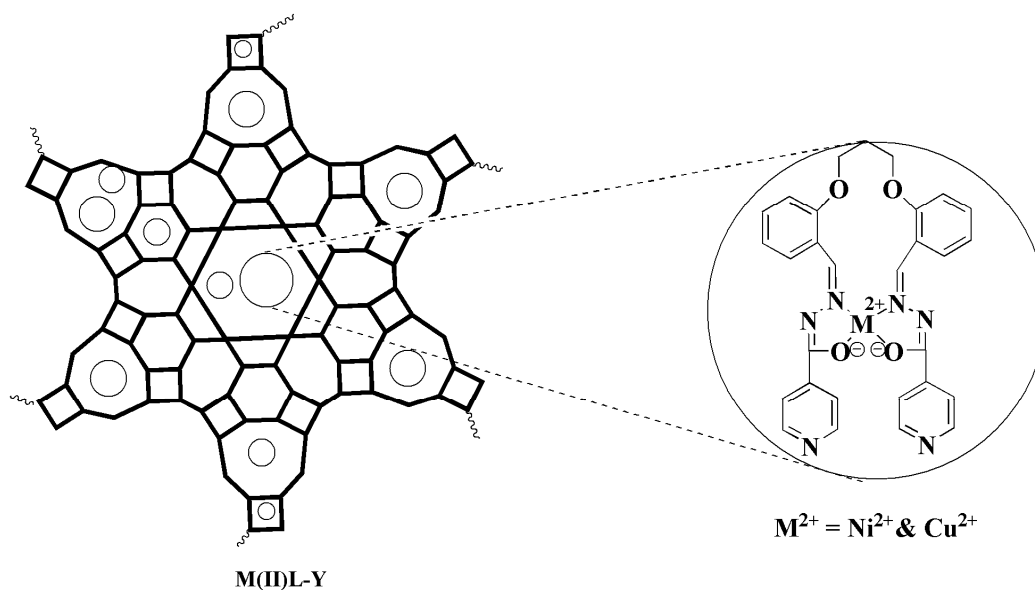817   **tetradentate N₂O₂ Schiff base moiety.**

818

819

820

821

822

M(II)L-Y

823   **Scheme (B): The proposed reaction mechanism and framework structure of zeolite with**

824   **encapsulated metal aryl hydrazone complexes of nickel (II) and copper(II).**